ORIGINAL RESEARCH

A Novel Grading System for Diffuse Chorioretinal Atrophy in Pathologic Myopia

Yu-Ning Niu · Hai-Long He · Xuan-Yu Chen · Sai-Guang Ling ·

Zhou Dong · Ying Xiong · Yue Qi · Zi-Bing Jin

ABSTRACT

Introduction: This study aims to quantitatively assess diffuse chorioretinal atrophy (DCA) in pathologic myopia and establish a standardized classification system utilizing artificial intelligence.

Methods: A total of 202 patients underwent comprehensive examinations, and 338 eyes were included in the study. The methodology involved image preprocessing, sample labeling, employing deep learning segmentation models, measuring and calculating the area and density of DCA lesions. Lesion severity of DCA was graded using statistical methods, and grades were assigned to describe the morphology of corresponding fundus photographs. Hierarchical clustering was employed to categorize diffuse atrophy fundus into three groups based on the area and density of diffuse atrophy (G1, G2, G3), while high myopic fundus without diffuse atrophy was designated as G0. One-way analysis of variance (ANOVA) and nonparametric tests were conducted to assess the statistical association with different grades of DCA.

Results: On the basis of the area and density of DCA, the condition was classified into four grades: G0, G1 ($0 <$ density ≤ 0.093), G2 ($0.093 <$ density ≤ 0.245), and G3 ($0.245 <$ density ≤ 0.712). Fundus photographs depicted a progressive enlargement of atrophic lesions, evolving from punctate-shaped to patchy with indistinct boundaries. DCA atrophy lesions exhibited a gradual shift in color from brown-yellow to yellow-white, originating from the temporal side of the optic disc and extending towards the macula, with severe cases exhibiting widespread distribution throughout the posterior pole. Patients with DCA were significantly older [34.00 (27.00, 48.00) vs 29.00 (26.00, 34.00) years], possessed a longer axial length (28.85 ± 1.57 vs 27.11 ± 1.01 mm), and exhibited a more myopic spherical equivalent [-13.00 (-16.00, -10.50) vs -9.09 ± 2.41 D] compared to those without DCA (G0) (all $P < 0.001$). In eyes with DCA, a trend emerged as grades increased from G1 to G3, showing associations with older age, longer axial length, deeper myopic spherical equivalent, larger area of parapapillary atrophy, and increased fundus tessellated density (all $P < 0.001$).

Yu-Ning Niu and Hai-Long He contributed equally to this work.

Y.-N. Niu · H.-L. He · Y. Xiong · Y. Qi · Z.-B. Jin (✉)
Beijing Institute of Ophthalmology, Beijing Tongren Eye Center, Beijing Tongren Hospital, Capital Medical University, Beijing 100005, China
e-mail: jinzibing@foxmail.com

X.-Y. Chen
Capital Medical University, Beijing 100069, China

S.-G. Ling · Z. Dong
EVision Technology (Beijing) Co. Ltd, Beijing 100085, China

Conclusions: The novel grading system for DCA, based on assessments of area and density, serves as a reliable measure for evaluating the severity of this condition, making it suitable for widespread application in the screening of pathologic myopia.

Keywords: Pathologic myopia; Diffuse chorioretinal atrophy; Artificial intelligence

Key Summary Points
Why carry out this study?
Diffuse chorioretinal atrophy (DCA) is recognized as the initial stage of pathologic myopia according to the International Photographic Classification and Grading System for Myopic Maculopathy (META-PM), playing a crucial role in its progression. Existing classification methods are relatively subjective and not easily comprehensible for beginners.
In this study, our objective is to quantitatively assess DCA in pathologic myopia and establish a standardized classification system using artificial intelligence.
What was learned from the study?
On the basis of the area and density of DCA, the condition was categorized into four grades: G0, G1 ($0 <$ density ≤ 0.093), G2 ($0.093 <$ density ≤ 0.245), and G3 ($0.245 <$ density ≤ 0.712).
The newly proposed grading system for DCA, based on assessments of area and density, renders it suitable for widespread application in the screening of pathologic myopia.

INTRODUCTION

Pathologic myopia, a leading cause of global irreversible blindness, particularly prevalent in Asia, has become one of the major causes of low vision in working-aged populations, as well as in the elderly population [1]. The prevalence of pathologic myopia has been progressively increasing over the years; a study demonstrated that by 2015, pathologic myopia accounted for approximately 0.13% of the global population, with an estimated projection of 55 million individuals affected by pathologic myopia worldwide by 2050 [2].

Myopic maculopathy is a prominent characteristic of pathologic myopia and represents the leading cause of irreversible visual impairment [3]. The International Photographic Classification and Grading System for Myopic Maculopathy (META-PM) categorizes myopic maculopathy into five distinct classes: no macular lesions (C0), tessellated fundus (C1), diffuse chorioretinal atrophy (DCA) (C2), patchy chorioretinal atrophy (C3), and macular atrophy (C4). Additionally, lacquer cracks, choroidal neovascularization (CNV), and Fuchs spot are considered "plus" signs [3]. According to this updated classification system, a pathologic myopia diagnosis is established when DCA and higher-grade lesions are present or posterior scleral staphyloma is present [3, 4]. The identification of DCA in the fundus serves as a crucial diagnostic indicator for pathologic myopia, playing a particularly significant role in its progression.

Diffuse chorioretinal atrophy represents one of the most prevalent pathological conditions associated with myopia and an early category of myopic maculopathy, the most common type of maculopathy in patients with pathological myopia [5, 6]. Importantly, the presence of DCA in childhood is more predisposed to developing new lesions of myopic maculopathy and progressing toward a more severe form of the condition [7–10]. Among children and adolescents with high myopia, a relatively high proportion exhibited the presence of DCA. Surprisingly, Jiang et al. [8] observed that 14.05% of the participants developed DCA during a follow-up

period exceeding 4 years, with the enlargement of DCA being identified as the primary progression pattern in myopic maculopathy. Similarly, Yokoi et al. [9] proposed that DCA around the optic disc in childhood serves as a pivotal predictor for the development of pathologic myopia in adulthood, highlighting the importance of early detection and diagnosis of DCA.

The appearance of DCA is characterized by a yellow-white lesion with an indistinct boundary located at the posterior pole of the eyeball, accompanied by blurred choroidal vessels within the atrophic area [10, 11]. The development of DCA has garnered significant attention from researchers, typically initiating from the temporal peripapillary region and subsequently expanding to encompass the entire deformed area of the posterior pole [12]. More significantly, DCA is highly susceptible to the progression of myopic retinopathy, leading to the emergence of a series of severe, vision-threatening lesions. Consequently, DCA is considered a progressive lesion closely associated with visual impairment [4].

The utilization of artificial intelligence technology in analyzing fundus images has reached a level where it can either compete with or approach the expertise of human specialists in automatically detecting various ophthalmic diseases [13, 14]. Advances in imaging processing technology now facilitate the quantitative measurement of DCA area and density through the analysis of fundus photographs. In this population-based observational study, we assessed the area and density of DCA, exploring their associations with ocular and systemic factors. On the basis of artificial intelligence image processing technology, we established a novel standardized quantitative evaluation system and objective grading criteria for DCA. These advancements aim to contribute to the clinical diagnosis of pathologic myopia by providing a more objective and standardized approach.

METHODS

Participants

In this retrospective observational study, we conducted a comprehensive analysis of patients at Beijing Tongren Hospital, Capital Medical University, diagnosed with high myopia by specialist ophthalmologists (YX and YQ). High myopia was defined as spherical equivalent ≤ -6.00 D and/or an axial length ≥ 26.0 mm. The study spanned from January 2022 to August 2023 and focused on individuals diagnosed with myopic maculopathy equal to diffuse chorioretinal atrophy (META-PM, C2). In order to conduct comparisons, we collected additional fundus images from patients diagnosed with high myopia but exhibiting META-PM at less than C2. Patients with myopic traction maculopathy and myopic macular neovascularization were excluded from the analysis. Exclusions also applied to individuals with combined ocular and systemic diseases, such as glaucoma, diabetic retinopathy, age-related degeneration, and retinal detachment. Additionally, cases with potential influences on the quantitative assessment of DCA, such as various types of cataracts, vitreous hemorrhage, and corneal opacity, were excluded.

This study received approval from the Ethics Committee of Beijing Tongren Hospital, and all procedures adhered to the principles outlined in the Declaration of Helsinki (TREC2022-KY045). Since this retrospective study involved noninvasive methods and deidentified data, informed consent was waived for study participants.

Examination

Demographic and clinical characteristics, including age and gender, were extracted from online medical records. All patients underwent routine ophthalmologic examinations, including assessments of visual acuity, intraocular pressure, and slit-lamp biomicroscopy. Fundus photography, captured using Topcon or Canon equipment, was conducted to encompass the macular and optic nerve head areas. Refraction

measurements, including cycloplegic and subjective refraction, were obtained, and best-corrected visual acuity (BCVA) was determined. Axial length (AL) measurements were taken using the IOL Master, A-mode ultrasonography, or LenStar devices. The spherical equivalent (SE) was calculated using the formula SE = spherical degrees + (cylindrical degrees/2). Fundus photographs were classified on the basis of the META-PM system (C2) by two experienced ophthalmologists (YNN and HLH), with any discrepancies resolved by a third experienced ophthalmologist (YQ).

AI Processing

The study utilizes intelligent fundus image analysis software, EVisionAI [15, 16], for processing fundus photographs. This software, meticulously designed to mimic the biomimetic mechanism of human vision, is specifically tailored to discern and extract diffuse features. Seamlessly integrating the characteristics of diffuse lesions across three facets (color channel, global scale, and local scale), EVisionAI enables the recognition and extraction of diffuse features in the specific region of myopic fundus. For each fundus photograph undergoing processing, a sequence of preprocessing operations, including region of interest (ROI) extraction, denoising, normalization, and enhancement, are initially conducted [17–19]. These operations aim to eliminate non-fundus structural areas to reduce the discrepancy between images, and increase internal feature differences in images, such as birth dates or left/right eye markings, which may hinder automated analysis of fundus images, impeding the identification and segmentation of DCA and potentially affecting subsequent disease recognition outcomes.

Following the preprocessing stage, a semantic segmentation network, TransUnet [20], based on Transformer architecture, is employed to delineate the diffuse feature regions. The preprocessed RGB images serve as inputs to the TransUnet network. The network initially employs the downsampling path of U-Net to extract features from the input image.

Subsequently, via Transformer modules, features from different scales are concatenated. The segmentation results are then generated using the upsampling path of U-Net. To galvanize the interplay of local and global information, the network incorporates skip connections, enabling the fusion of features from lower and higher levels, thereby improving segmentation performance. TransUnet adroitly synthesizes the strengths of both convolutional neural networks (CNN) and Transformer, exhibiting the computational efficiency of CNN and the capability for capturing global contextual information inherent to Transformer. Compared to other lesions, DCA typically exhibits larger and more extensive areas with irregular shapes and variable locations within the fundus. CNN-based models alone often struggle to capture these distinguishing features effectively, leading to missed detections of these larger lesion areas. By integrating information from the three channels, the model demonstrates enhanced recognition and segmentation of diffuse feature regions.

Regarding the model samples, two medical professionals independently annotated a comprehensive collection of 2694 sample images. One individual conducted the initial annotations, while the other engaged in rigorous review and corrections. The dataset was divided into training and testing sets in a 7:3 ratio. The training set samples were utilized to train the TransUnet network model. The accuracy of model segmentation was evaluated using the test set. The accuracy, sensitivity, and specificity were calculated at the pixel level, resulting in values of 0.997, 0.978, and 0.998, respectively. Subsequently, on the basis of the segmented diffuse feature regions, the study quantitatively computed the area of diffuse atrophy and diffuse atrophy area per unit area of the fundus (diffuse lesion density, DLT) [16, 19] (Fig. 1). As shown in Fig. 1, the heatmap deviates from the conventional Grad-CAM map. Instead, it is a schematic diagram constructed from the segmented DCA region and fundus tessellation. First, segmentation models yield both the fundus tessellation and DCA regions. Subsequently, the area of fundus tessellation undergoes mean filtering to derive a density map. This density

map is then combined with the DCA region and transformed into a color image using the JET colormap to present the visualization with high matching accuracy. Furthermore, instead of processing each channel individually, a three-channel convolution is employed to merge the three-channel image into a single channel. The convolution weights are learned during training, capturing information from all three channels simultaneously.

Statistical Analysis

Statistical analyses were conducted using IBM SPSS Statistics 26 for Windows (IBM SPSS Statistics, USA) and R software. Hierarchical clustering was employed to categorize diffuse atrophy fundus into three groups based on the area of diffuse atrophy (G1, G2, G3), while high myopic fundus without diffuse atrophy was designated as G0. To assess the normality of variables, the Kolmogorov–Smirnov test was applied to G0, G1, G2, and the entire dataset ($N > 50$), whereas the Shapiro–Wilk test was used for G3 ($N \leq 50$). Variables confirmed to follow a normal distribution were presented using the mean and standard deviation, while non-normally distributed variables were described using the median and interquartile range.

For comparing differences among the four groups, a one-way analysis of variance (ANOVA) was utilized for variables exhibiting normal distribution, while non-normally distributed variables were subjected to nonparametric tests. Gender differences were assessed using the chi-square test. All P values were two-sided, and a significance level of $P < 0.05$ was considered statistically significant.

RESULTS

Baseline Characteristics

In the study, a total of 338 eyes from 202 participants underwent examination and were included in the final analysis. The mean age was 31.00 (26.00, 41.00) years (range 13–77 years). The mean AL was 27.73 (26.95, 29.06) mm (range 24.16–33.05 mm). The mean SE was -11.00 (-14.00, -8.50) D (range -25.50 to -2.50 D). The mean area of DCA in all eyes was
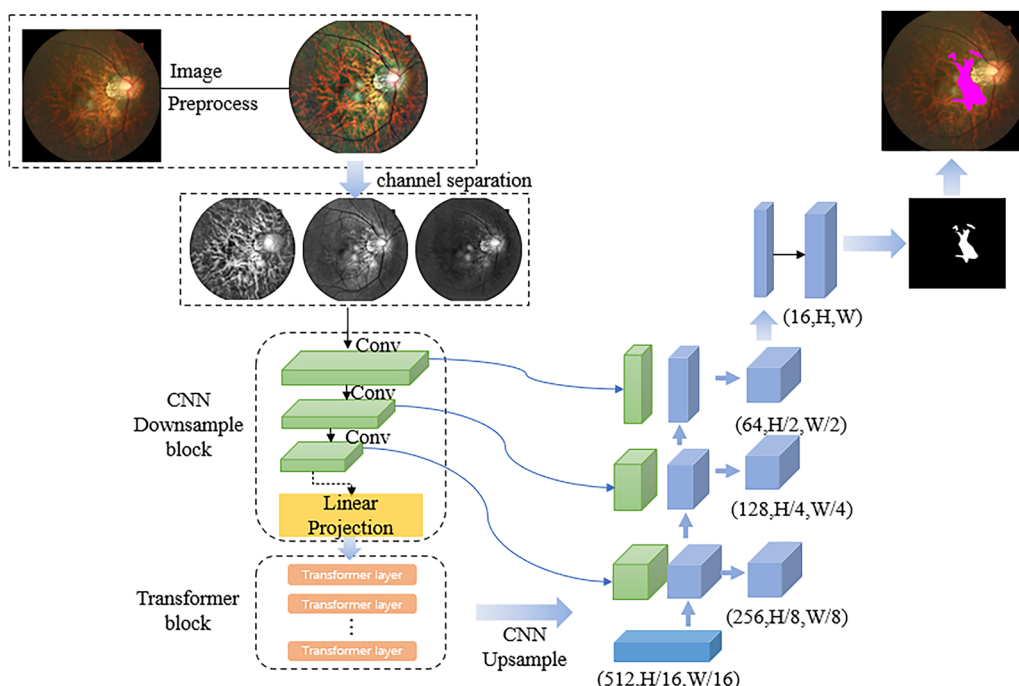

Fig. 1 Flowchart of diffuse chorioretinal atrophy by artificial intelligence technology. *CNN* convolutional neural networks

9,494,497 (3,734,401, 20,438,918) μm^2, with a range from 6688 to 77,894,083 μm^2. The mean area of parapapillary atrophy was 2,489,770 (1,657,660, 4,236,180) μm^2, ranging from 1,657,660 to 4,236,180 μm^2. The mean fundus tessellated density (FTD) was 0.331 (0.251, 0.399), with a range from 0.063 to 0.536. Among these eyes, a total of 266 belonged to female participants, accounting for 78.70%. The participant distribution revealed that 57.69% had DCA (G1–G3), while 42.31% had none DCA (G0) (Table 1).

Proposed Classification and Definition of DCA

Utilizing artificial intelligence, we employed advanced deep learning techniques to discern and quantify the extent and density of lesions associated with DCA through the analysis of fundus images. This approach enabled us to establish quantitative indicators, thereby characterizing the distinctive patterns of lesions evident in these images.

DCA was categorize into four groups based on area (G0, G1, G2, G3). Eyes without DCA were designated as grade 0 (G0). The DCA area gradually increased from grade 1 (G1) to grade 3 (G3). A total of 143 (42.31%) eyes were categorized as G0, 101 (29.88%) eyes as G1, 61 (18.05%) eyes as G2, and 33 (9.76%) eyes as G3. The mean area of DCA at G1 level was 3,917,756 (1,692,014, 6,735,617) μm^2, range from 6688 to 10,170,786 μm^2. The density of DCA at G1 level was $0.000 < \text{density} \leq 0.093$. The mean area of DCA at G2 level was $17,230,214 \pm 4,621,804$ μm^2, range from 10,441,332 to 27,034,940 μm^2. The density of DCA at G2 level was $0.095 < \text{density} \leq 0.245$. The mean area of DCA at G3 level was 41,624,143 (33,195,894, 50,114,161) μm^2, range from 29,412,464 to 77,894,083 μm^2. The density of DCA at G3 level was $0.245 < \text{density} \leq 0.712$. This allowed us to assign the severity of DCA into four categories: "non-DCA" (G0), "mild DCA" (G1), "moderate DCA" (G2), and "severe DCA" (G3). To maintain continuity of data within the novel classification methodology, values situated within discontinuous intervals will be reassigned to the subsequent categorical level. Corresponding images and detailed descriptions of these categories are provided in Fig. 2 and Table 2, offering a comprehensive visual and textual representation of the diverse manifestations of DCA.

Comparison of Associated Factors Between Eyes with and Without DCA

Table 1 presents a demographic comparison between G0 and G1–G3. The patients with DCA (G1–G3) were significantly older than those without DCA (G0) ($P < 0.001$). The mean age for participants without DCA (G0) was 29.00 (26.00, 34.00) years, whereas for those with DCA it was 34.00 (27.00, 48.00) years, with an overall age range of 13.00 to 77.00 years. No statistically significant differences in gender were observed between the groups ($P = 0.977$). Eyes with DCA exhibited a significantly longer AL (28.85 ± 1.57 mm) compared to those without DCA (27.11 ± 1.01 mm), and eyes with DCA showed a more myopic SE [$- 13.00$ ($- 16.00$, $- 10.50$) D] than G0 ($- 9.09 \pm 2.41$ D) ($P < 0.001$).

Comparison of Associated Factors Among Eyes with Different Grades of DCA

The demographic features and ocular biometry for each DCA grade are detailed in Table 3. There was a trend for participants to be older, have longer AL, and have more myopic SE as DCA developed (all $P < 0.001$). No statistically significant difference was found for gender ($P = 0.977$).

Table 3 presents the parapapillary atrophy area and fundus tessellated density for the different DCA grades. As DCA developed, the parapapillary atrophy area also increased ($P < 0.001$). The mean fundus tessellated density increased from 0.260 ± 0.079 in G0 to 0.350 ± 0.078 in G1 and further to 0.414 ± 0.048 in G2. However, the mean fundus tessellated density decreased from 0.414 ± 0.048 in grade 2 to 0.381 (0.310, 0.416) in G3 ($P < 0.001$).

Table 1 Comparisons of characteristics between eyes with and without DCA

	Total	G0	G1–G3	P value
No. of eyes (%)	338	143	195	
Age, years				
Mean ± SD	31.00 (26.00, 41.00)	29.00 (26.00, 34.00)	34.00 (27.00, 48.00)	< 0.001
Range	13.00 to 77.00	13.00 to 55.00	20.00 to 77.00	
N	338	143	195	
Gender				
M/F	72/266	29/114	43/152	0.977
N	338	143	195	
Spherical equivalent, D				
Mean ± SD	− 11.00 (− 14.00, − 8.50)	− 9.09 ± 2.41	− 13.00 (− 16.00, − 10.50)	< 0.001
Range	− 25.50 to − 2.50	− 16.00 to − 2.50	− 25.50 to − 3.75	
N	336	143	193	
Axial length, mm				
Mean ± SD	27.73 (26.95, 29.06)	27.11 ± 1.01	28.85 ± 1.57	< 0.001
Range	24.16 to 33.05	24.16 to 31.23	25.17 to 33.05	
N	307	135	172	

DCA diffuse chorioretinal atrophy, *SD* standard deviation, *D* diopter

Distribution of DCA Based on AL and SE

To further investigate the distribution patterns of DCA, participants were subdivided into three groups based on AL and SE. The incidence of DCA displayed an upward trend with longer AL, rising from 13.3% in eyes with an AL ≤ 26.00 mm to 84.3% in eyes with an AL > 28.00 mm. Within each AL interval, G1 lesions accounted for the highest proportion of DCA, followed by G2, with G3 lesions having the lowest occurrence. The likelihood of higher-grade DCA increased with the elevation in DCA grade, especially within longer Al intervals. Each DCA type demonstrated a higher probability of distribution in longer AL intervals, with G1, G2, and G3 (51.14%, 81.48%, and 96.67%, respectively) being predominantly distributed in the AL interval > 28 mm. Notably, the majority of G3 lesions (96.67%) were found within the range of AL > 28 mm (Fig. 3a).

Similar to AL, the proportion of DCA increased with more myopic SE, ranging from 20.63% in eyes with SE > − 8.00 D to 94.12% in eyes with SE ≤ − 14.00 D. Among all DCA grades, G1 exhibited the highest frequency (65.66%) within the range of − 14.00 < SE ≤ − 8.00 D, G2 showed the greatest prevalence (50.82%) for SE ≤ − 14.00 D, and G3 demonstrated the most pronounced distribution (81.82%) in the SE ≤ − 14.00 D range. This comprehensive analysis illuminates the correlation between DCA incidence and both AL and spherical equivalent, providing valuable insights into the associations between ocular parameters and the development of DCA (Fig. 3b).
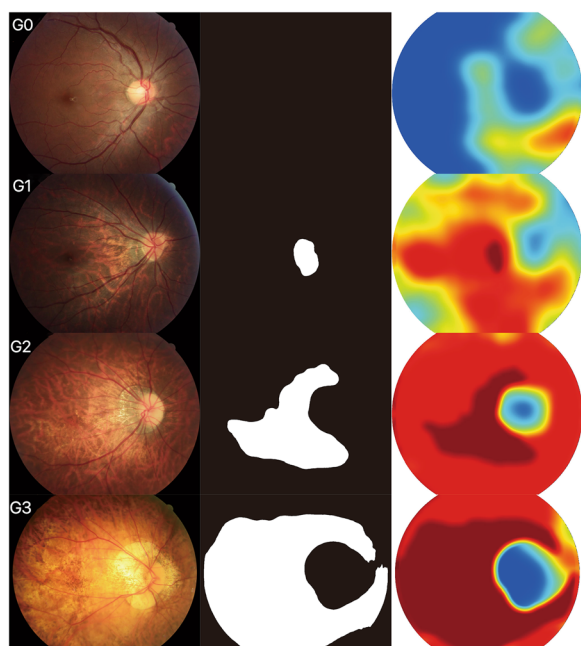
Fig. 2 Extraction of diffuse chorioretinal atrophy by artificial intelligence technology of G0 (non-diffuse chorioretinal atrophy), G1 (mild diffuse chorioretinal atrophy), G2 (moderate diffuse chorioretinal atrophy), and G3 (severe diffuse chorioretinal atrophy)

DISCUSSION

To the best of our knowledge, this study is the first to quantitatively measure DCA on fundus photographs through the utilization of artificial intelligence image processing technology and statistical methods. Notably, our research makes a novel contribution by precisely identifying and quantifying the atrophy area of DCA, presenting a novel approach to classifying DCA severity on the basis of both area and density. This study unveils the extent and characteristics of atrophic changes in DCA lesions of pathologic myopia. In previous studies, Ohno-Matsui et al. employed a two-phase approach to propose META-PM for myopic maculopathy [3]. The initial phase involved conducting a consensus meeting to formulate a classification system. Subsequently, the second phase encompassed the assessment of inter- and intraobserver agreement in applying this classification system to a set of 100 selected fundus photographs. In our research, we have

innovatively employed artificial intelligence image processing techniques and statistical methods to establish the novel classification.

Initially, we identified three articles that comprehensively proposed classifications for DCA in detail. In 2019, Fang et al. conducted swept-source optical coherence tomography (SS-OCT) examinations on a total of 747 eyes with DCA and quantified the choroidal thickness (CT) at five specific points located below and 3 mm away from the fovea, including nasal, temporal, superior, and inferior regions. Two distinct subtypes were identified on the basis of the regional thinning pattern in choroidal thickness: peripheral DCA (PDCA) and macular DCA (MDCA). Moreover, considering the progressive nature of these lesions, a critical diagnostic threshold was proposed for distinguishing PDCA from MDCA [21]. In 2020, Liu and colleagues further advanced the grading of DCA by ETDRS (Early Treatment of Diabetic Retinopathy Study) grid to fundus photographs. The choroid layer is categorized into four grades (D0–D3) based on lesion location and extent [22]. Furthermore, Park and colleagues utilized an ultra-wide-angle fundus camera to capture red (633 nm) and green (532 nm) separation images of the nipple and macular reflectance covering the extent of increase. DCA was classified into four levels, with each level's lesion form described in detail [23]. Although current research on DCA classification has made significant strides in terms of detail and objectivity, limitations persist as a result of the subjective nature of clinical diagnosis based on fundus photographs. Therefore, our proposed classification system relies on artificial intelligence for identifying the area and density of DCA lesions through deep learning analysis of fundus images.

The advantage of this study is that it is the first quantitative study of DCA by latest artificial intelligence extraction quantitative technology to quantitatively grade DCA based on the acquired area and density of DCA. Our study employed statistical methodologies to categorize the DCA area and density, followed by an analysis of the associated factors within each category. The progression and prognosis of DCA in pathologic myopia can be predicted on the

Table 2 Proposed classification of diffuse chorioretinal atrophy

	Area (mm^2)	Density	Clinical defining features
Grade 0	0	0	No diffuse chorioretinal atrophy lesions; or lesions were not identified by artificial intelligence
Grade 1	0 < area ≤ 10.170786	0.000 < density ≤ 0.093	The atrophic lesions were located in the temporal region of the optic disc, exhibiting indistinct boundaries and a punctate distribution pattern. The fovea within the macular area remained unaffected by these lesions. Within these areas of atrophy, choroidal vascular structures appeared significantly blurred or absent, often displaying perivascular circumferential involvement
Grade 2	10.170786 < area ≤ 27.034940	0.093 < density ≤ 0.245	The atrophic lesions exhibited large yellow-white sheets with indistinct margins, frequently localized around the optic disc, and involved the fovea. However, these lesions generally did not extend beyond the temporal aspect of the macula. Choroidal vascular structure was disrupted or absent within the atrophic lesions
Grade 3	27.034940 < area ≤ 77.894083	0.245 < density ≤ 0.712	The yellowish-white atrophy lesions exhibit indistinct borders and are widely distributed throughout the eye. Within the atrophic areas, the choroidal blood vessel structure completely vanishes

basis of the size, density, and ocular biological characteristics of DCA.

Furthermore, our study specifically focused on evaluating distinct regions within the macula and optic disc using various partitioning methods, enabling a more comprehensive understanding of the distribution and characteristics of a specific region in relation to DCA. In G1 and G2, the lesions were predominantly localized in the temporal side of the optic disc, with fewer observed in the nasal side of the optic disc and the temporal region of the macula. Upon reaching G3, atrophic lesions were distributed throughout the entire posterior pole of the eyeball. Our study aligns with previous findings regarding the association between pathologic myopia and choroidal thickness. Curtin's observation [24] of choroidal changes in eyes with pathologic myopia revealed varying degrees of thinning in different regions of the posterior pole of the eyeball. The most obvious thinning trend was observed on the temporal side of the optic disc (a decrease by 53.5%), while the nasal side exhibited the least thinning trend (a decrease by 39.2%). Notably, among all regions, the area between the optic disc and fovea demonstrated significant thinning.

In our population-based study, we analyzed risk factors associated with the degree of DCA in 338 eyes within the high myopia population. Strong statistical correlations were observed with larger age, longer AL, and deeper SE, which resulting in higher degree of DCA. Additionally, a significant correlation was found between a larger parapapillary atrophy area, increased fundus tessellated density, and the degree of DCA classification. Respectively, the average age

Table 3 Basic characteristics of different grade of DCA

Characteristic	Grade 0	Grade 1	Grade 2	Grade 3	*P* value
No. of eyes (%)	143	101	61	33	
Age, years					
Mean ± SD	29.00 (26.00, 34.00)	31.00 (26.00, 41.00)	36.00 (27.00, 48.00)	47.85 ± 11.87	< 0.001
Range	13.00 to 55.00	20.00 to 68.00	21.00 to 77.00	22.00 to 70.00	
N	143	101	61	33	
Gender					
M/F	29/114	22/79	14/47	7/26	0.977
N	143	101	61	33	
Spherical equivalent, D					
Mean ± SD	− 9.09 ± 2.41	− 11.69 ± 2.93	− 14.43 ± 4.38	− 17.22 ± 4.27	< 0.001
Range	− 16.00 to − 2.50	− 17.50 to − 5.75	− 24.00 to − 3.75	− 25.50 to − 8.50	
N	143	99	61	33	
Axial length, mm					
Mean ± SD	27.11 ± 1.01	28.04 ± 1.24	29.38 ± 1.40	30.26 ± 1.30	< 0.001
Range	24.16 to 31.23	25.17 to 31.77	26.91 to 33.05	26.94 to 32.42	
N	135	88	54	30	
Area of DCA, μm^2					
Mean ± SD	0	3,917,756 (1,692,014, 6,735,617)	17,230,214 ± 4,621,804	41,624,143 (33,195,894, 50,114,161)	< 0.001
Range	0	6688 to 10,170,786	10,441,332 to 27,034,940	29,412,464 to 77,894,083	
N	143	101	61	33	
Area of PPA, μm^2					
Mean ± SD	1,817,750 (1,211,815, 2,474,785)	2,814,300 (1,919,290, 3,905,450)	4,497,940 (3,245,750, 7,220,230)	9,535,377 ± 5,069,671	< 0.001
Range	0 to 6,567,680	0 to 16,251,900	757,959 to 13,262,200	1,549,690 to 20,389,600	
N	143	101	61	33	
Fundus tessellated density					
Mean ± SD	0.260 ± 0.079	0.350 ± 0.078	0.414 ± 0.048	0.381 (0.310, 0.416)	< 0.001
Range	0.063 to 0.479	0.124 to 0.536	0.318 to 0.523	0.113 to 0.497	
N	143	101	61	33	

DCA diffuse chorioretinal atrophy, *SD* standard deviation, *PPA* peripapillary atrophy, *D* diopter, *N* number of eyes
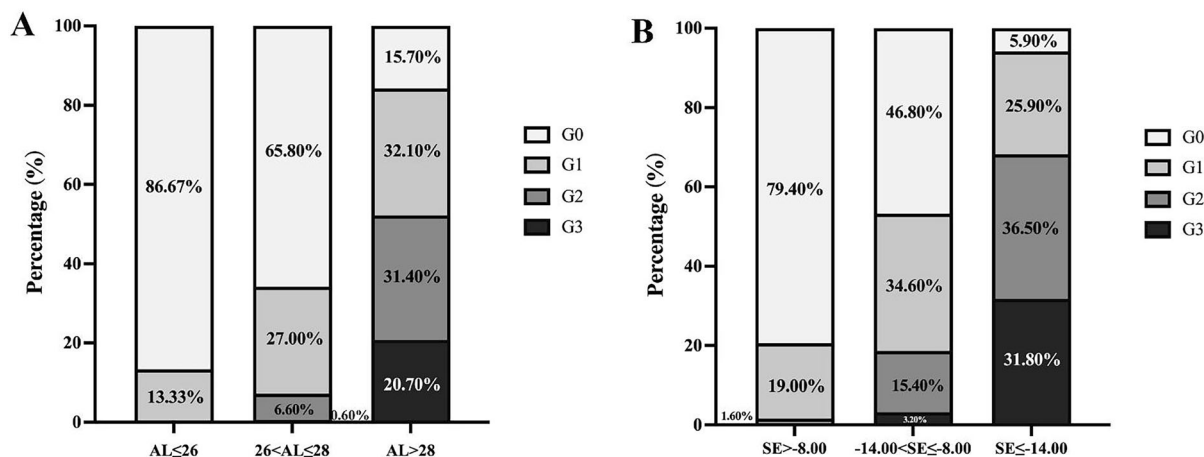
Fig. 3 Distribution of DCA based on **a** axial length and **b** spherical equivalent. *DCA* diffuse chorioretinal atrophy, *AL* axial length, *SE* spherical equivalent

of patients with G0–G3 was 29.00 (26.00, 34.00), 31.00 (26.00, 41.00), 36.00 (27.00, 48.00), and 47.85 ± 11.87 years. Therefore, the average age increased from G0 to G3 with the severity of the disease. This aligns with previous research demonstrating a decrease in choroidal thickness with age. Notably, age has been identified as the most influential factor in the development of DCA [21]. Furthermore, a significant association was observed between DCA and AL as well as SE, indicating that deeper SE and longer AL were more predisposed to high-grade DCA. The prevalence of DCA was also investigated on the basis of AL intervals, revealing that the majority of eyes with DCA had an AL greater than 28 mm (84.3%), with most SE falling in the range of 14.00 < SE ≤ − 8.00 D (51.81%). These results suggest a higher degree of myopia, longer AL, and choroidal thinning due to mechanical forces in eyes with DCA. The results of Tian et al. in a study of 206 eyes with varying degrees of myopic atrophic maculopathy suggest that DCA was the dominant myopic atrophic maculopathy grade in eyes with myopic tractional maculopathy [25]. The application of longer AL may contribute to increased mechanical tensile strength, potentially facilitating the formation and progression of DCA.

We also examined the relationship between DCA and optic disc morphological characteristics. The results show that larger parapapillary

atrophy area was associated with the progression of DCA. Previously, several studies have shown that progression of myopic maculopathy is associated with increased area of parapapillary atrophy [26, 27]. Meanwhile, Chen et al. showed that eyes with larger parapapillary atrophy areas had significantly thinner choroidal thickness [28].

Additionally, we investigated the association between DCA and FTD. Previous research by Shao et al. demonstrated that FTD can be used as a quantitative biomarker to evaluate the choroidal thickness in the general population [18]. In our study, the majority of fundus images with DCA exhibited varying degrees of FTD. Therefore, investigating the trend of FTD in different stages of DCA is crucial for physicians to assess the severity of DCA and also holds significant implications for unraveling its pathogenesis. In this study, we employed image processing to quantitatively measure FTD in the eyes of patients with pathologic myopia, revealing that fundus tessellated density initially increased and subsequently decreased as DCA progressed. The mean fundus tessellated density values escalated from 0.260 ± 0.079 at stage 0 to 0.350 ± 0.078 in grade 1, further rising to 0.414 ± 0.048 in grade 2; however, it declined to 0.381 (0.310, 0.416) in grade 3 instead. This finding suggests that FTD decreases when DCA reaches a certain level of severity. Thus, this result indicates that the lesions may

have reached an advanced degree when distinct areas of retinal thinning are observable in fundus photographs but tessellation abnormalities are not easily discernible. This observation is consistent with the results of previous studies. He et al., on the basis of fundus tessellated density in 403 eyes, observed a decreasing trend in FTD with an increasing pathologic myopia category [16]. This can be explained by the thinning of choroidal traction in DCA, narrowing or disappearance of numerous choroidal capillary contractions, decreased choroidal capillary density, and decreased blood flow circulation resulting in photoreceptor apoptosis, which becomes difficult or impossible to observe because of the absence of retinal pigment epithelium and choroidal capillaries [29].

There are some limitations. Firstly, despite including a larger DCA sample, the study was conducted in an ophthalmology clinic at a single center and included only Asian populations, which may limit the applicability of DCA area classification levels to non-Asian populations. Secondly, the thickness of the choroid, a key factor in the diagnosis of diffuse chorioretinal atrophy, was not subjected to a detailed comparative analysis at all levels of DCA. Such an analysis could provide a more comprehensive understanding of DCA lesions and contribute to a more accurate diagnosis of DCA. Thirdly, our study primarily relies on artificial intelligence image processing and statistical methods to establish a novel classification. The prospective clinical application and validation of this classification system necessitates subsequent multicenter clinical cohort studies and trials in the future to ensure broader generalizability and thorough testing in real-world clinical settings.

CONCLUSION

Our study has established a standardized quantitative assessment system and objective grading criteria for DCA using artificial intelligence. We have elucidated the developmental trends of DCA through comprehensive analysis of fundus photographs at all stages, providing an effective means for the clinical evaluation of

pathologic myopia. Early detection, diagnosis, and treatment are crucial in reducing the incidence of myopia-related blindness and implementing timely interventions for pathologic myopia.

REFERENCES

1. Ohno-Matsui K, Wu PC, Yamashiro K, et al. IMI pathologic myopia. Invest Ophthalmol Vis Sci. 2021;62(5):5.

2. Fricke TR, Jong M, Naidoo KS, et al. Global prevalence of visual impairment associated with myopic macular degeneration and temporal trends from 2000 through 2050: systematic review, meta-analysis and modelling. Br J Ophthalmol. 2018;102(7): 855–62.

3. Ohno-Matsui K, Kawasaki R, Jonas JB, et al. International photographic classification and grading system for myopic maculopathy. Am J Ophthalmol. 2015;159:877–83 (e877).

4. Ohno-Matsui K, Lai TY, Lai CC, et al. Updates of pathologic myopia. Prog Retin Eye Res. 2016;52: 156–87.

5. Hayashi K, Ohno-Matsui K, Shimada N, et al. Long-term pattern of progression of myopic maculopathy: a natural history study. Ophthalmology. 2010;117(8):1595–611 (1611.e1-4).

6. Okoro T. Atlas of posterior fundus changes in pathologic myopia. Tokyo: Springer; 1998. p. 5–22.

7. Ohno-Matsui K. Insights into childhood myopic maculopathy. JAMA Ophthalmol. 2024. https://doi.org/10.1001/jamaophthalmol.2023.6490.

8. Jiang F, Wang D, Xiao O, et al. Four-year progression of myopic maculopathy in children and adolescents with high myopia. JAMA Ophthalmol. 2024. https://doi.org/10.1001/jamaophthalmol.2023.6319.

9. Yokoi T, Jonas JB, Shimada N, et al. Peripapillary diffuse chorioretinal atrophy in children as a sign of eventual pathologic myopia in adults. Ophthalmology. 2016;123(8):1783–7.

10. Holden BA, Fricke TR, Wilson DA, et al. Global prevalence of myopia and high myopia and temporal trends from 2000 through 2050. Ophthalmology. 2016;123:1036–42.

11. Liu HH, Xu L, Wang YX, et al. Prevalence and progression of myopic retinopathy in Chinese adults: the Beijing Eye Study. Ophthalmology. 2010;117:1763–8.

12. Tokoro T. Explanatory factors of chorioretinal atrophy. NewYork: Springer; 1998. p. 25–50.

13. Long E, Lin H, Liu Z, et al. An artificial intelligence platform for the multihospital collaborative management of congenital cataracts. Nat Biomed Eng. 2017;1: 0024.19.

14. Koutsouleris N, Kambeitz-Ilankovic L, Ruhrmann S, et al. Prediction models of functional outcomes for individuals in the clinical high-risk state for psychosis or with recent-onset depression: a multimodal, multisite machine learning analysis. JAMA Psychiat. 2018;75:1156–72.

15. Liu F, Yu XH, Wang YC, et al. Quantitative analysis of optic disc changes in school-age children with ametropia based on artificial intelligence. Int J Ophthalmol. 2023;16(11):1727–33.

16. He HL, Liu YX, Chen XY, et al. Fundus tessellated density of pathologic myopia. Asia Pac J Ophthalmol (Phila). 2023;12(6):604–13.

17. Xu Y, Ling SG, Dong Z, et al. Development and application of a fundus image quality assessment system based on computer vision technology. Chin J Ophthalmol. 2020;56:920–7.

18. Shao L, Zhang QL, Long TF, et al. Quantitative assessment of fundus tessellated density and associated factors in fundus images using artificial intelligence. Transl Vis Sci Technol. 2021;10(9): 23–23.

19. Long T, Xu Y, Zou H, et al. A generic pixel pitch calibration method for fundus camera via automated ROI extraction. Sensors (Basel). 2022;22(21): 8565.

20. Zhang Y, Li Z, Nan N, et al. TranSegNet: hybrid CNN-vision transformers encoder for retina segmentation of optical coherence tomography. Life (Basel). 2023;13(4):976.

21. Fang Y, Du R, Nagaoka N, et al. OCT-based diagnostic criteria for different stages of myopic maculopathy. Ophthalmology. 2019;126(7):1018–32.

22. Liu R, Guo X, Xiao O, et al. Diffuse chorioretinal atrophy in Chinese high myopia: the ZOC-BHVI high myopia cohort study. Retina. 2020;40(2): 241–8.

23. Park UC, Lee EK, Yoon CK, et al. Progression pattern of myopic maculopathy according to the severity of DCA and choroidal thickness. Sci Rep. 2022;12(1): 3099.

24. Curtin BJ, Karlin DB. Axial length measurements and fundus changes of the myopic eye. I. The posterior fundus. Trans Am Ophthalmol Soc. 1970;68: 312–34.

25. Tian J, Qi Y, Lin C, et al. The association in myopic tractional maculopathy with myopic atrophy maculopathy. Front Med (Lausanne). 2021;20(8): 679192.

26. Yan YN, Wang YX, Yang Y, et al. Ten-year progression of myopic maculopathy: the Beijing eye study 2001–2011. Ophthalmology. 2018;125: 1253–63.

27. Fang Y, Yokoi T, Nagaoka N, et al. Progression of myopic maculopathy during 18-year follow-up. Ophthalmology. 2018;125:863–77.

28. Chen Q, He J, Yin Y, et al. Impact of the morphologic characteristics of optic disc on choroidal thickness in young myopic patients. Invest Ophthalmol Vis Sci. 2019;60:2958–67.

29. Cheng T, Deng J, Xu X, et al. Prevalence of fundus tessellation and its associated factors in Chinese children and adolescents with high myopia. Acta Ophthalmol. 2021;99(8):e1524–33.